TITLES OF SUPPLEMENTAL MATERIALS

Supplemental **Figure S1-7**. Relevant to Figures 1-7.

Figure S1. Quantitative analysis of cellular proteome remodeling in response to AA withdrawal and MTOR inhibition. Relevant to Figure 1.

Figure S2. TEX264 is localized in the ER and is trafficked into autophagosomes upon nutrient stress prior to degradation in the lysosome. Relevant to Figure 2.

Figure S3. Generation of TEX264$^{-/-}$ cells reconstituted with TEX264-eGFP, and LIR-dependent association of TEX264 with autophagy machinery upon starvation. Relevant to Figure 3.

Figure S4. TEX264 accumulates in ATG8-positive punctate structures at ER tubule 3-way junctions followed by fusion with lysosomes. Relevant to Figure 4.

Figure S5. Characterization of ER stress response in TEX264$^{-/-}$ cells. Relevant to Figure 6.

Figure S6. A role for TEX264 in ER-phagy revealed by quantitative proteomics. Relevant to Figure 6.

Figure S7. TEX264 status determines ER-phagic flux. Relevant to Figure 7.

Supplemental **Table S1**. Global proteomics for autophagy-dependent proteome remodeling. Relevant to Figures 1 and S1.

Supplemental **Table S2**. TMT-based interaction and proximity biotinylation proteomics for TEX264. Relevant to Figure 3 and 5.

Supplemental **Table S3**. Global proteomics reveals TEX264 as a major ER-phagy regulator. Relevant to Figure 6.

Supplemental **Table S4**. Ranked relative abundance of the ER proteins whose abundance is altered in a TEX264, ATG7, or RB1CC1-dependent manner in response to AA withdrawal. Relevant to Figure 6.

Supplementary Figure S1

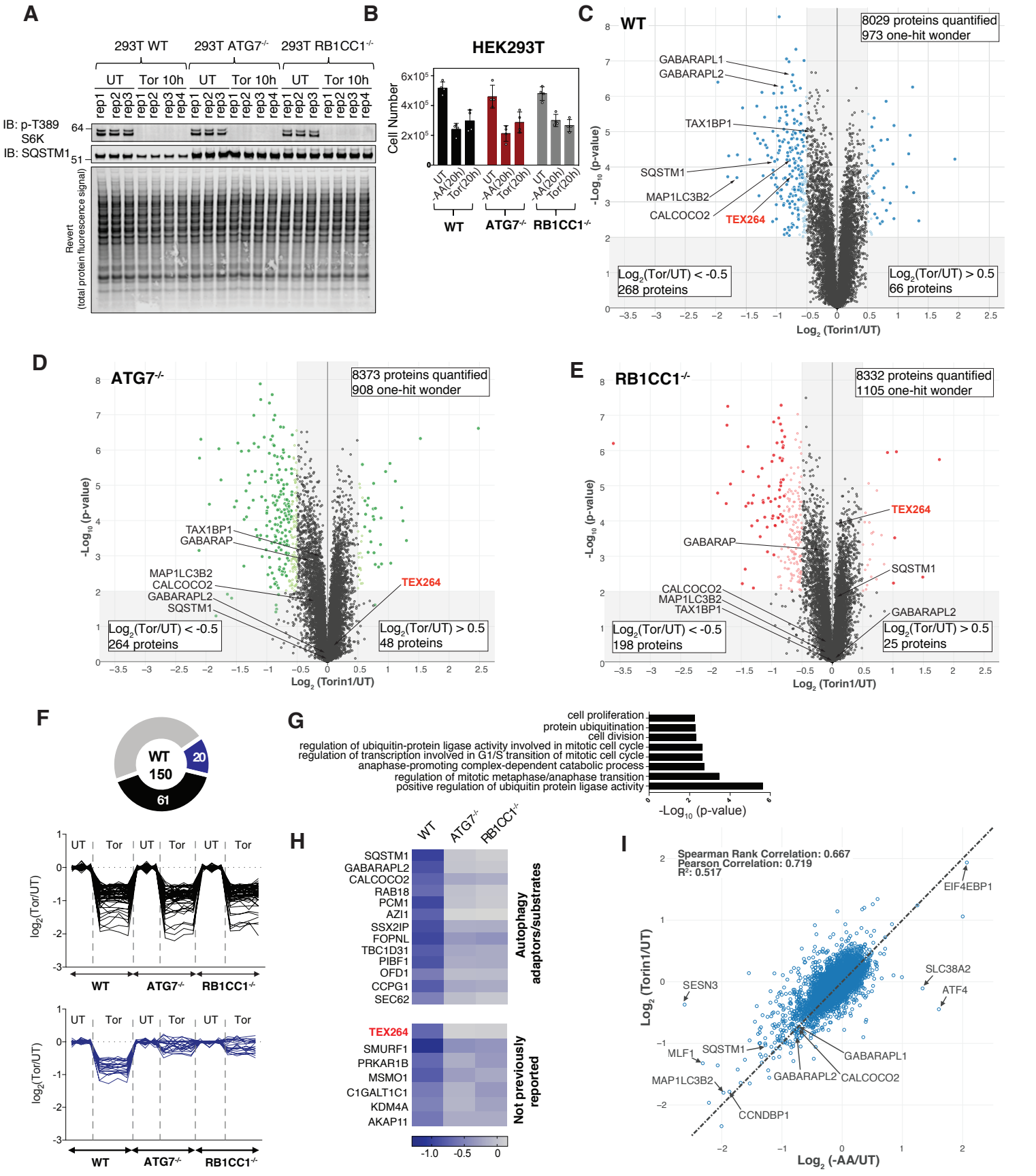

Figure S1. Quantitative analysis of cellular proteome remodeling in response to AA withdrawal and MTOR inhibition. Related to Figure 1.

(A) Immunoblotting of extracts used for TMT proteomics. The indicated cells were treated with Torin1 (Tor, 150 nM, 10h) and whole cell extracts subjected to immunoblotting with the indicated antibodies.

(B) Cell proliferation analysis of the indicated cells after either AA withdrawal (20h) or treatment with Torin1 (150 nM, 20h).

(C-E) Volcano plots -Log_{10} p-value versus Log_2-ratio of Torin1/UT for 293T WT, ATG7$^{-/-}$, or RB1CC1$^{-/-}$ cells as described in panel A. Proteins with Log_2(Torin1/UT) < -0.5 or > 0.5 (p-value <0.01) are indicated as colored empty circles, and filled colored circles indicate statistically significant hits (Welch's t-test (S0 = 0.585), corrected for multiple comparison by permutation-based FDR (5%)).

(F) Total 150 proteins passed filters of Log_2(Torin1/UT) < -0.5 in WT HEK293T cells, detected in all three genotypes (p<0.01), and more than 2 peptides quantified. Log_2(Tor/UT) values for 61 individual proteins (black plot) whose abundance was reduced (p<0.01) by log_2(Tor/UT) <-0.5 across WT, ATG7$^{-/-}$ and RB1CC1$^{-/-}$ cells. Also, Log_2(Tor/UT) values for 20 individual proteins (blue plot) whose abundance was reduced (p<0.01) by log_2(Tor/UT) <-0.5 in WT cells but not in ATG7$^{-/-}$ and RB1CC1$^{-/-}$ cells. These 20 proteins showed more than 30% abundance difference between WT and ATG7$^{-/-}$.

(G) Gene ontology (GO) analysis of 61 proteins from panel F using DAVID GO analysis (top plot).

(H) Heat map of Log_2(Tor/UT) values for 20 individual proteins from panel F (lower plot).

(I) Correlation plot between proteins whose abundance is reduced in response to either AA withdrawal or Torin1 treatment. Comparisons are made from data in **Table S1**.

Supplementary Figure S2

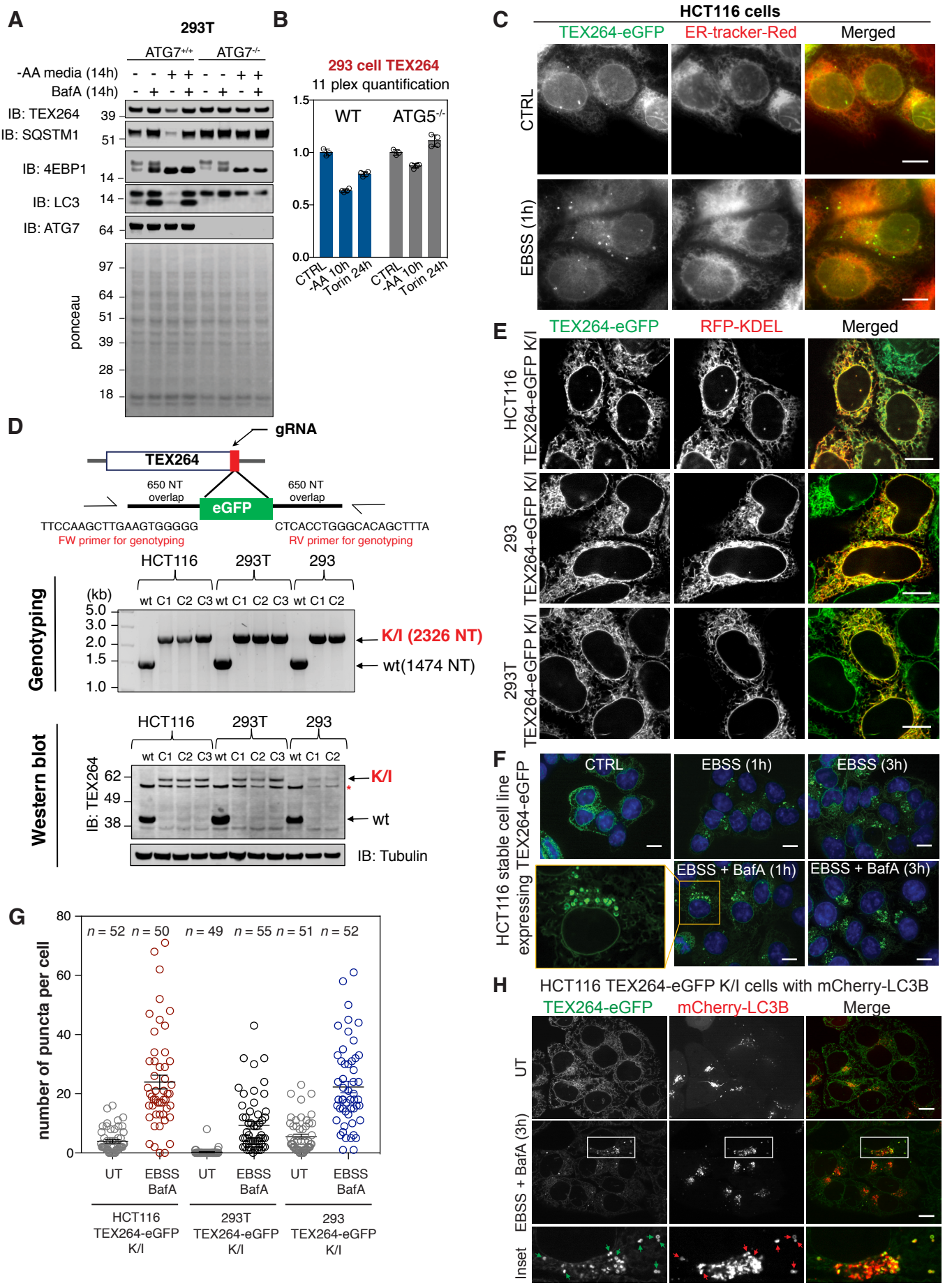

Figure S2. TEX264 is localized in the ER and is trafficked into autophagosomes upon nutrient stress prior to degradation in the lysosome. Related to Figure 2.

(A) The indicated 293T cells with or without ATG7 were left untreated or subjected to AA withdrawal in the presence or absence of BafA (25 nM, 14h). Whole cell extracts were subjected to immunoblotting with the indicated antibodies.

(B) TMT based quantification of TEX264 abundance in 293 cells with or without ATG5 in response to AA withdrawal (10h) or MTOR inhibition with Torin1 (150 nM, 24h). Error bars represent SD for triplicate or quadruplicate measurements.

(C) HCT116 cells stably expressing TEX264-eGFP (2.4-fold over endogenous levels) and ER-tracker Red to mark the ER were imaged using wide-field microscopy. Scale bar = 10 μm.

(D) Gene editing of 293T, 293, and HCT116 cells using CRISPR-Cas9 to fuse eGFP with the C-terminus of TEX264. Homozygous incorporation of eGFP was confirmed by genotyping using the indicated primers. Extracts from the indicated cells were subjected to immunoblotting with the indicated antibodies. Note that the TEX264 expression level is suppressed after the endogenous tagging.

(E) The indicated TEX264 knock-in (K/I) cells were transfected with vectors expressing RFP-KDEL to mark ER and imaged by confocal microscopy. Scale bar = 10 μm.

(F) HCT116 cells stably expressing TEX264-eGFP (2.4-times the endogenous level) were either left untreated or were subjected to starvation for the indicated times in the presence or absence of BafA (25 nM) prior to imaging with confocal microscopy. Scale bar = 10 μm.

(G) Quantification of TEX264-eGFP puncta in HCT116 TEX264-eGFP knock-in cells that were either left untreated or incubated in EBSS and BafA (25 nM) for 3h. A cut off size of 0.7 microns in diameter was used for determination of puncta number. Error bars = SEM for ~50 cells.

(H) HCT116 TEX264-eGFP knock-in cells expressing mCherry-LC3B were either left untreated or were subjected to starvation in the presence of BafA (3h) prior to imaging with confocal microscopy. Scale bar = 10 μm.

Supplemental Figure S3

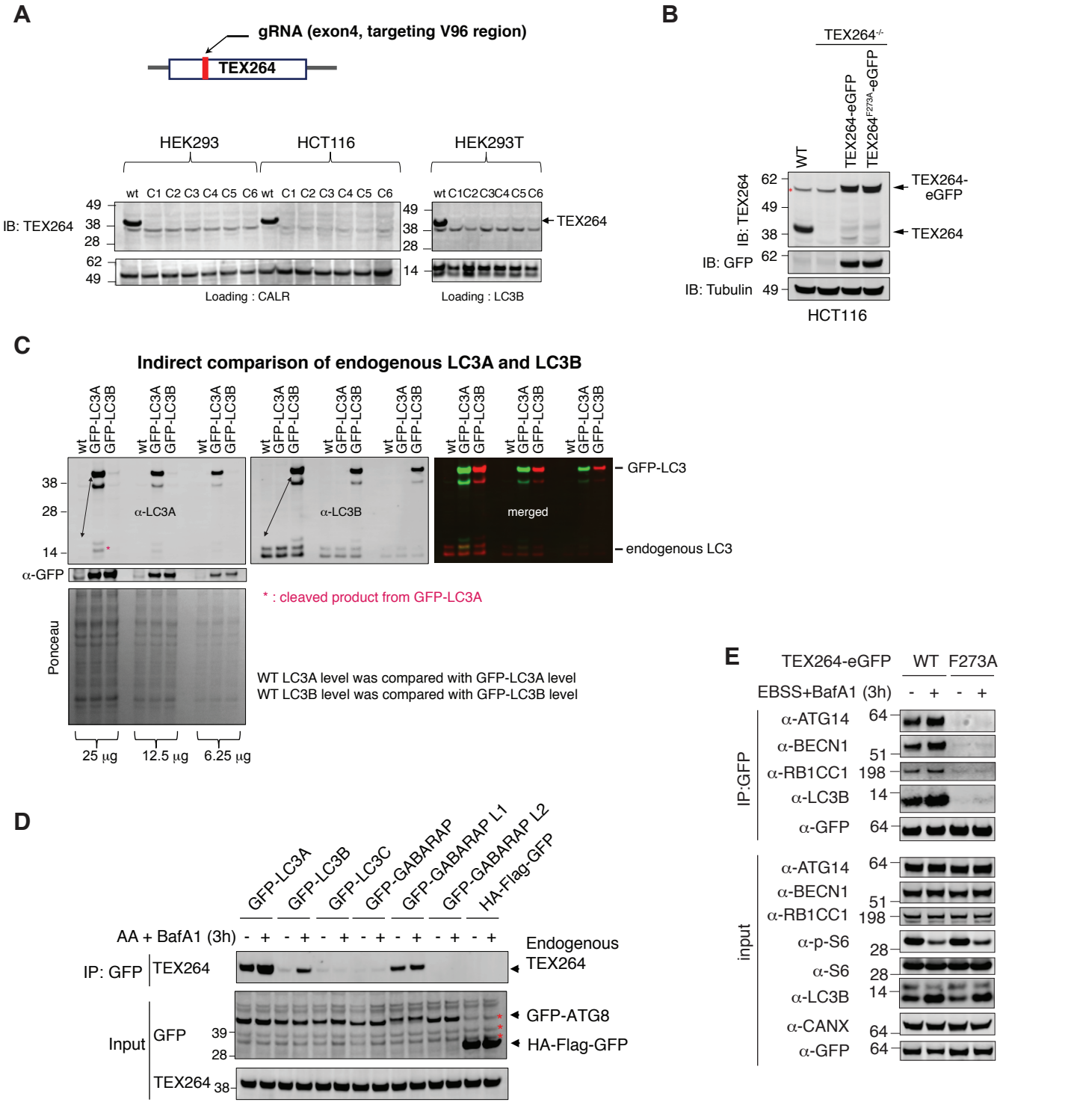

Figure S3. Generation of TEX264$^{-/-}$ cells reconstituted with TEX264-eGFP, and LIR-dependent association of TEX264 with autophagy machinery upon starvation. Related to Figure 3.

(A) Immunoblotting of extracts of 293T, 293 and HCT116 cell clones after gene editing with a CRISPR-Cas9 gRNA targeting exon 4 to create null alleles. Note that LC3B-I and II level did not change in TEX264$^{-/-}$ cells suggesting the general autophagy flux was not altered by TEX264 deletion.

(B) HCT116 TEX264$^{-/-}$ cells were reconstituted with a lentivirus stably expressing TEX264-eGFP or TEX264^{F273A}-eGFP and cell extracts analyzed by immunoblotting. Asterisk (red) indicates a non-specific band.

(C) HCT116 cells expressing equal levels of eGFP-LC3A or eGFP-LC3B (obtained by flow sorting) were lysed and 15, 16.5, or 6.25 μg of whole cell extracts from these cells as well as HCT116 cells without eGFP-LC3 expression were subjected to immunoblotting with antibodies specific for LC3A or LC3B. With equal levels of signal for the expressed eGFP fusion protein (as measured with α-GFP), we then visualized endogenous LC3A or B, finding that under conditions where LC3B is readily detectable in HCT116 cells, LC3A was at or below the limit of detection.

(D) HCT116 cells were infected with lentiviruses expressing GFP-tagged ATG8 proteins or HA-Flag-GFP as a control. Cells were sorted to identify populations with equivalent levels of GFP protein expression. Anti-GFP immune complexes were immunoblotted with the indicated antibodies.

(E) Extracts from HCT116$^{-/-}$ cells expressing TEX264-eGFP or TEX264^{F273A}-eGFP were subjected to immunoprecipitation with α-GFP prior to immunoblotting with the indicated antibodies. Cell extracts (input) were used for positive controls.

Supplementary Figure 4

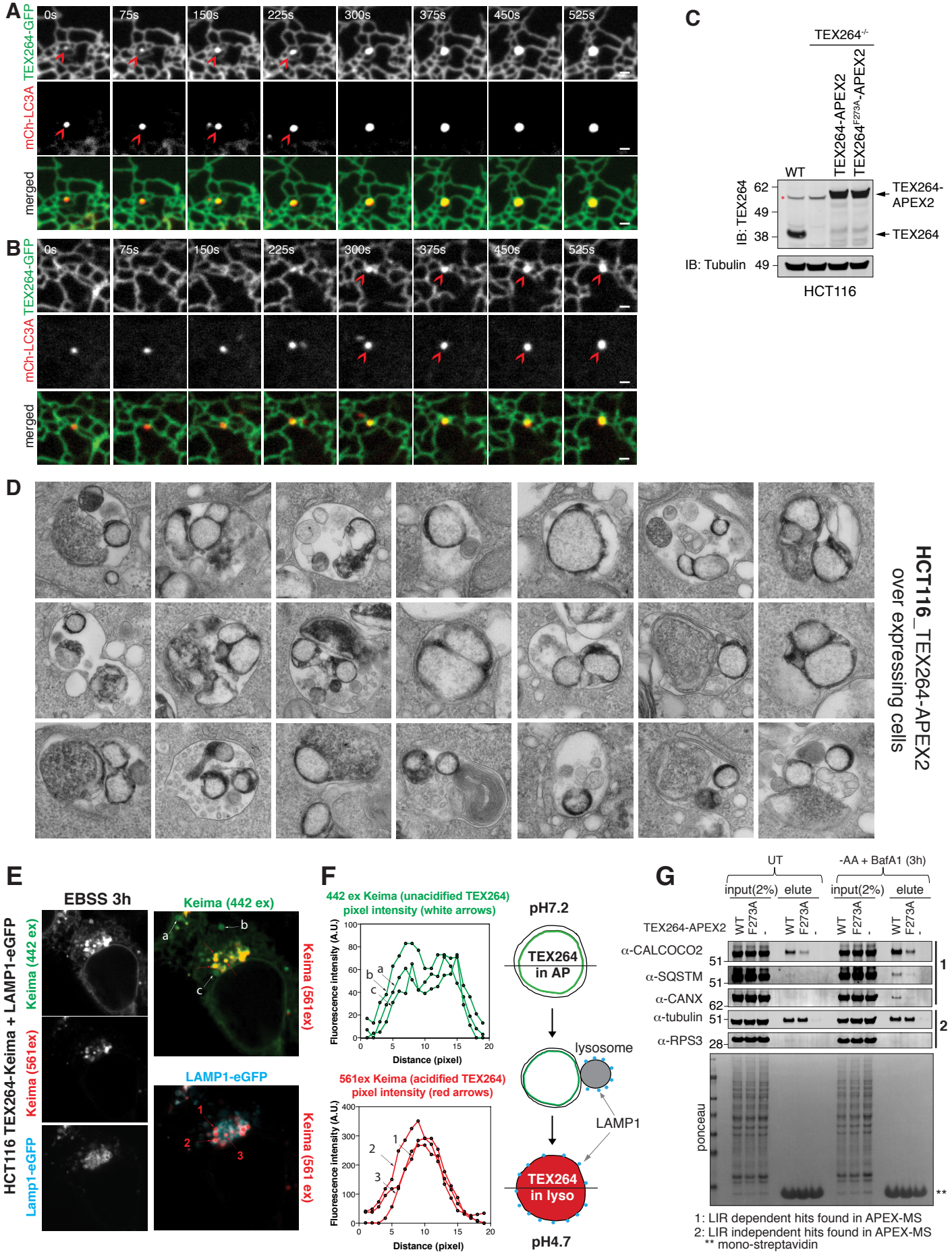

Figure S4. TEX264 accumulates in ATG8-positive punctate structures at ER tubule 3-way junctions followed by fusion with lysosomes. Related to Figure 4.

(A,B) COS7 cells stably expressing TEX264-eGFP and mCherry-LC3A were subjected to live-cell confocal imaging during starvation. Two examples (panels A and B) of time-lapse images of individual regions of the cell cortex containing an LC3A-positive punctate structure located at a ER tubule 3-way junction are shown. Scale bar = 1 μm.

(C) HCT116 TEX264$^{-/-}$ cells were reconstituted with a lentivirus expressing either TEX264-APEX2 or TEX264^{F273A}-APEX2. Extracts from cells were subjected to immunoblotting with the indicated antibodies. Asterisk (red) indicates a non-specific band.

(D) TEX264-APEX2 analysis of cells after EBSS plus BafA treatment for 3h using DAB staining and EM of cell thin sections. In this experiment, TEX264-APEX2 was transiently overexpressed for 48h prior to analysis.

(E,F) Examination of TEX264-Keima in autophagosomes and lysosomes. HCT116 TEX264-Keima cells expressing LAMP1-eGFP were subjected to nutrient stress (EBSS) for 3h prior to imaging by confocal microscopy (panel E). Fluorescence intensity in a cross-section of individual vesicles displaying only 442nm excitation (white arrows) is plotted in panel F (top), while that of 561nm excitation (red arrows) is plotted in F (bottom). A schematic model (right) describes how the shape of the fluorescence intensity across vesicles allows interpretation of TEX264 positive autophagosomal structures and fusion with lysosomes.

(G) HCT116 cells expressing TEX264-APEX2 or TEX264^{F273A}-APEX2 were either left untreated or subjected to AA withdrawal for 3h (+BafA). Cells were treated with biotin tyramide (30 min) and H_2O_2 (1.5 min), then the biotinylated proteins purified using streptavidin beads. Purified proteins or crude lysates were immunoblotted with the indicated antibodies.

Supplementary Figure S5

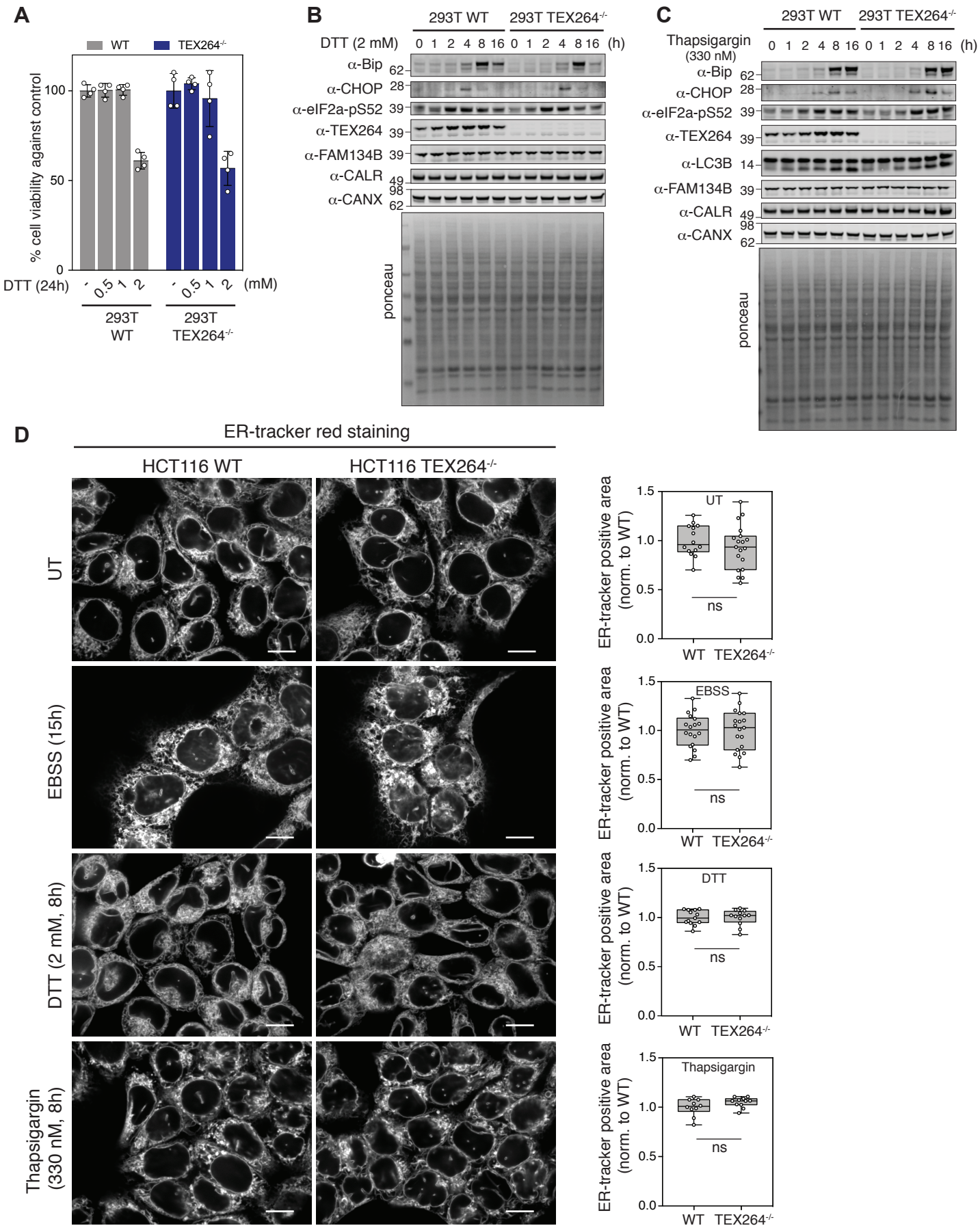

Figure S5. Characterization of ER stress response in TEX264$^{-/-}$ cells. Related to Figure 6.

(A) Cell viability of WT and TEX264$^{-/-}$ HCT116 cells 24h after treatment with DTT (0-2 mM). Viability was measured using trypan blue. Data are represented as mean ± SD for quadruplicate measurements.

(B, C) WT and TEX264$^{-/-}$ 293T cells were treated with either DTT (2 mM) or Thapsigargin (330 nM) for the indicated time periods prior to analysis of cell extracts by immunoblotting.

(D) WT and TEX264$^{-/-}$ HCT116 cells were either left untreated (UT) or treated with EBSS, DTT (2 mM) or Thapsigargin (330 nM) for the indicated time periods prior to analysis of cells using ER-tracker red and imaging. ER-tracker-positive area/cell was determined as described in the method section and signals normalized to WT.

Supplementary Figure S6.

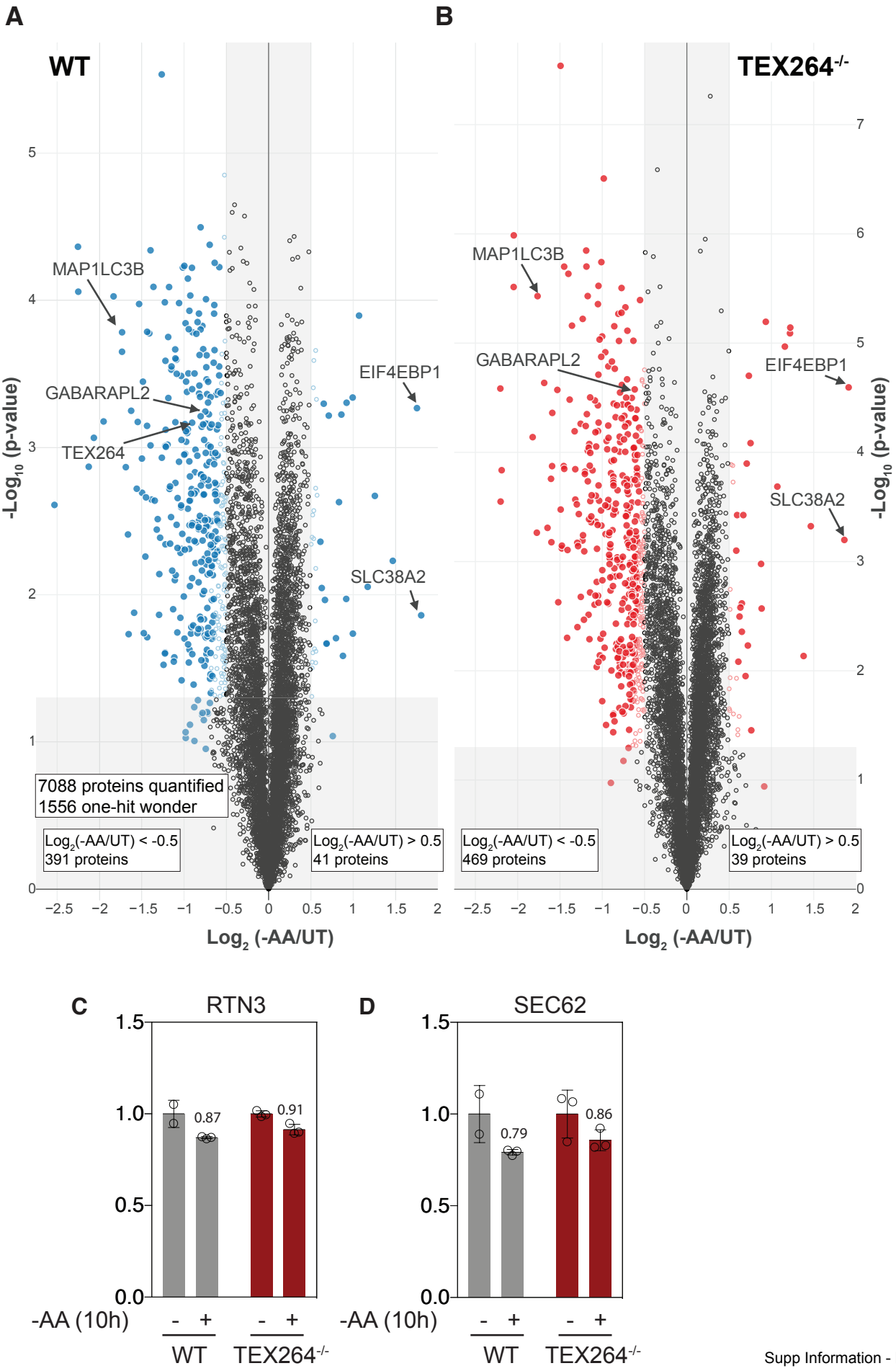

Figure S6. A role for TEX264 in ER-phagy revealed by quantitative proteomics. Related to Figure 6.

(A, B) Volcano plots for $-Log_{10}$ (p-value) versus Log_2(-AA/UT) (A) for WT cells or (B) for TEX264$^{-/-}$ cells. Proteins with Log_2(-AA/UT) < -0.5 or > 0.5 (p-value <0.05) are indicated as colored empty circles, and filled colored circles indicate statistically significant hits (Welch's t-test (S0 = 1), corrected for multiple comparison by permutation-based FDR (1%)).

(C, D) Relative abundance of RTN3 and SEC62 in WT or TEX264$^{-/-}$ cells in response to AA withdrawal (10h). Error bars are SD for duplicate or triplicate measurements for peptides from RTN3 and SEC62.

Supplementary Figure S7

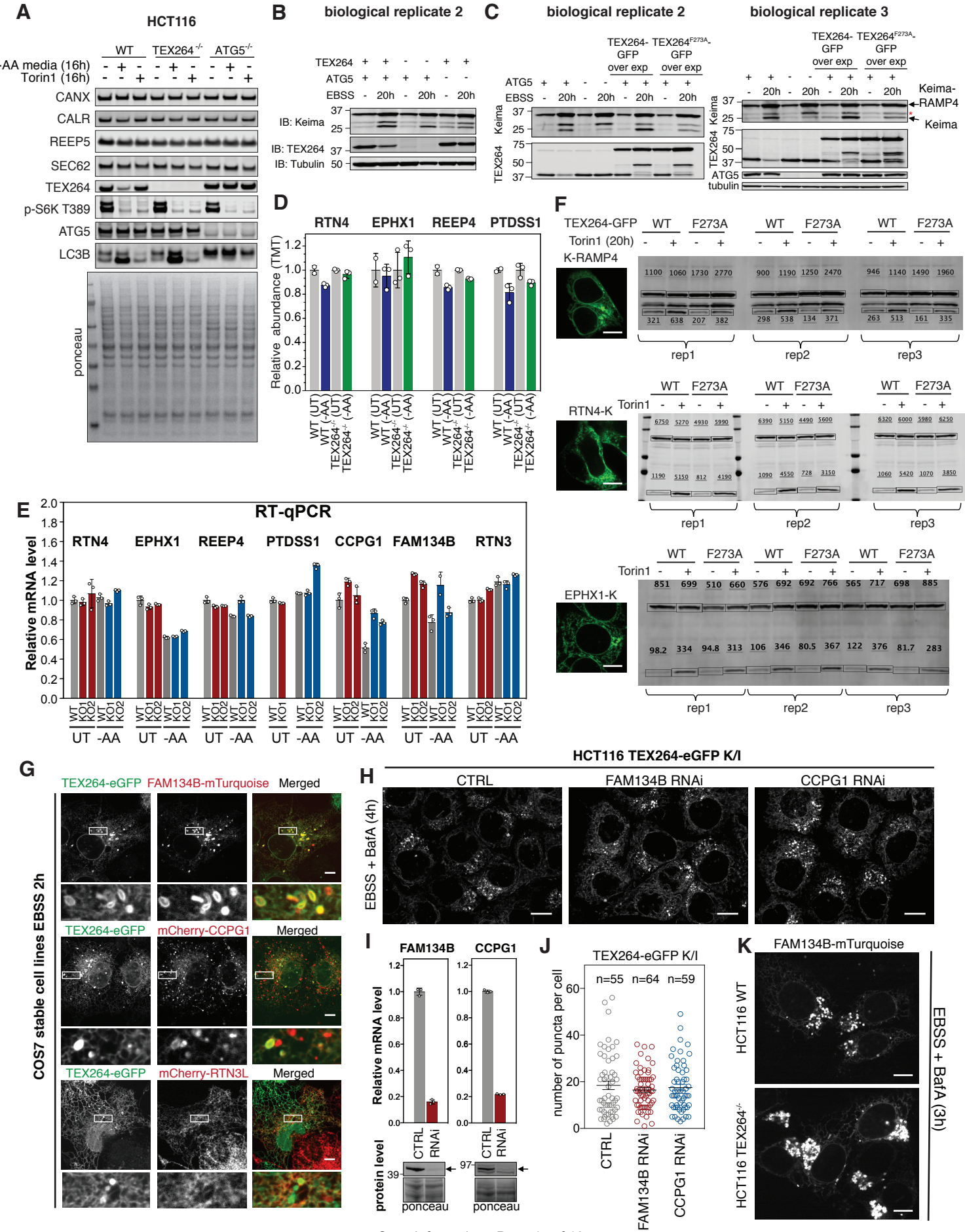

Figure S7. TEX264 status determines ER-phagic flux. Related to Figure 7.

(A) The indicated HCT116 cells were subjected to either Torin1 treatment or AA withdrawal (16h) and total cell extracts subjected to immunoblotting with the indicated antibodies.

(B) Cells lacking TEX264 display reduced ER-phagic flux. HCT116 WT or TEX264$^{-/-}$ cells expressing the Keima-RAMP4 ER-phagy reporter were sorted by flow-cytometry to equalize the expression level. The cells were either left untreated or subjected to starvation (EBSS, 20h) and cell extracts analyzed for Keima-RAMP4 and "processed" Keima using immunoblotting. This is replicate 2 compared with the data in Figure 7.

(C) Overexpression of TEX264 promotes ER-phagy. HCT116 cells (WT or ATG5$^{-/-}$) expressing Keima-RAMP4 and either TEX264-eGFP or TEX264^{F273A}-eGFP were left untreated or subjected to starvation (EBSS, 20h). Cell extracts were examined for Keima-RAMP4 and "processed" Keima by immunoblotting. This is replicate 2 and 3 compared with the data in Figure 7.

(D) Relative abundance (TMT-MS^3) of the indicated proteins in WT or TEX264$^{-/-}$ cells in response to AA withdrawal (10h). Error bars are SD for duplicate or triplicate measurements for all identified peptides for each protein. Data are derived from Table S3.

(E) qPCR demonstrates that the mRNA abundance for the indicated ER proteins is largely unaffected by deletion of TEX264 in HCT116 cells with or without nutrient stress (10h, AA withdrawal).

(F) Analysis of ER-phagic flux using Keima-RAMP4, RTN4-Keima and EPHX1-Keima in HCT116 TEX264$^{-/-}$ cells reconstituted with either TEX264^{WT} or TEX264^{F273A}. Left panel: Confocal imaging of HCT116 cells stably expressing the indicated ER protein fused with Keima. Scale bar = 10 μm. Right panel: α-Keima immunoblots showing triplicate assays for Keima processing in response to MTOR inhibition with Torin1 (16h). Signal quantification processed by ImageStudioLite is labeled on the blot image. These data were used to generate histograms shown in Figure 7F.

(G) COS7 cells stably expressing the indicated fluorescent proteins were subjected to starvation (EBSS) for 2h prior to imaging by confocal microscopy. Scale bar = 10 μm.

(H) HCT116 TEX264-eGFP K/I cells were transfected with the indicated siRNA and 52h post transfection, were subjected for EBSS (+BafA) treatment followed by live cell imaging analysis.

(I) RT-qPCR indicates that mRNA abundance for FAM134B and CCPG1 reduced to 16% and 21%, respectively, 52h after the siRNA transfection as in panel H, and the corresponding proteins level decreased accordingly.

(J) Number of puncta per cell quantification of images in panel H is shown as a scatter plot. Error bars = SEM for >50 cells.

(K) HCT116 WT or TEX264$^{-/-}$ cells stably expressing FAM134B-mTurquoise were subjected to starvation in the presence of BafA (3h) prior to imaging by confocal microscopy. Scale bar = 10 μm.

Supplemental Tables and Movies Legend

Table S1. Global proteomics for autophagy-dependent proteome remodeling. TMT data for total proteomes of 293T cells (either untreated, -AAs for 10h, or treated with Torin1 for 10h) [Sheet 1], 293T cells deleted for ATG7 (either untreated, -AAs for 10h, or treated with Torin1 for 10h) [Sheet 2], or 293T cells deleted for RB1CC1 (either untreated, -AAs for 10h, or treated with Torin1 for 10h) [Sheet 3]. Relevant to Figure 1 and S1.

Table S2. TMT-based interaction and proximity biotinylation proteomics for TEX264. TMT data for a-GFP immune complexes from cells expressing TEX264-eGFP comparing either WT versus F273A mutant of TEX264 [Sheet 1] and streptavidin purification of biotinylated peptides as described in Figure 5A [Sheet 2]. Relevant to Figure 5.

Table S3. Global proteomics reveals TEX264 as a major ER-phagy regulator. TMT-based global proteomics data for cells with or without TEX264 with or without AA withdrawal [Sheet 1]. Relevant to Figure 6.

Table S4. Ranked relative abundance of the ER proteins whose abundance is altered in a TEX264, ATG7, or RB1CC1-dependent manner in response to AA withdrawal. Abundance change of each protein was normalized to untreated cells for each genotype. Relevant to Figure 6.

Movie S1. Visualization of ER tubules marked by TEX264-eGFP (green) and autophagosomes marked by mCherry-LC3A in COS7 cells after AA withdrawal. Movie was taken 1h post EBSS addition. Relevant to Figure 4.

Movie S2. Visualization of ER tubules marked by TEX264-eGFP (green) and lysosomes marked by Lysotracker-Red in COS7 cells after EBSS treatment. Movie was taken 1h post-EBSS addition. Relevant to Figure 4.